31st Annual International Conference of the IEEE EMBS
Minneapolis, Minnesota, USA, September 2-6, 2009

Magnetic Resonance Electric Property Imaging of Brain Tissues

Xiaotong Zhang, *Student Member, IEEE*, Shanan Zhu, and Bin He, *Fellow, IEEE*

Abstract— **The electric properties (EPs) of brain tissues, i.e., the electric conductivity and permittivity, can provide important information for diagnosis of various brain disorders. A high-field MRI system is accompanied by significant wave propagation effects, and the radio frequency (RF) radiation is dependent on EPs of the biological tissue. Based on the measurement of the active transverse magnetic component of the applied RF field (known as B1-mapping technique), we have developed a dual-excitation algorithm, which uses two sets of measured B1 data, to noninvasively reconstruct the biological tissue's electric properties. A series of computer simulations were conducted to evaluate the feasibility and performance of the proposed method on a 3-D head model within a birdcage coil and a transverse electromagnetic coil. Compared with other B1-mapping based reconstruction algorithms, our approach provides superior performance without the need for iterative computations. The present simulation results indicate good reconstruction of electric properties of brain tissues from noninvasive MRI B1 mapping.**

I. Introduction

The electric properties (EPs, conductivity σ and permittivity ε) of biological tissues at radio and microwave frequencies have been the subject of research for over four decades [1]. In the past two decades, many efforts have been made to produce cross-sectional images of EPs *in vivo* by means of the Electrical Impedance Tomography (EIT) [2] and its variants using magnetic induction (MIT) [3]. However, these methods are limited by low spatial resolution due to the surface voltage measurements and the need to solve an ill-posed inverse problem. A technique called "Magnetic Resonance Electrical Impedance Tomography (MREIT)" [4], which is based on the Magnetic Resonance Current Density Imaging (MRCDI) [5] technique and measures current injection inducted MR phase shifts, has been pursued; but it requires current injection into the body within an MRI scanner. Another recently developed approach, Magnetoacoustic Tomography with Magnetic Induction (MAT-MI) [6], suggests the promises of obtaining high resolution tissue electrical conductivity profiles; however, there are no *in vivo* experiments reported so far.

In 1991, Haacke et al. proposed a method of extracting EPs from MRI images [7]. By using an iterative sensitivity-matrix algorithm, these authors suggested that the EPs can be estimated using MRI images which reflect the disrupted RF profile. Later on, Wen reported a modified Helmholtz equation based non-iterative algorithm and tested in phantom experiments on 1.5T and 4.7T MRI [8]. Recently, using an iterative algorithm derived from Ampere's Law, Katscher et al. conducted an *in vivo* experiment on a 3T MRI system to image the EPs within a human head and leg [9].

The B_1-mapping technique was developed to measure the rotating RF field components: the transmitted and received field in RF coils [10,11]. With the principle of reciprocity [12], the Cartesian transverse component of the RF magnetic field, H_x and H_y, can be derived. MREPT utilizes these two measurements to reconstruct the EP values within the biological tissues, and it differs from other noninvasive imaging techniques in that no electrode mounting is required and no external energy is introduced into the body during MRI scanning. It can be performed on a standard MRI system using a regular volume coil, and its spatial resolution is determined by MRI images and the quality of the applied B_1-mapping technique.

In the present study, we have developed a new non-iterative dual-excitation algorithm to image the tissue EPs by means of MREPT, and conducted computer simulation studies to evaluate its performance. The performance of the proposed MREPT algorithm is evaluated using a five-tissue 3-D realistic head model, a shielded 12-rung birdcage and transverse electromagnetic (TEM) coil.

II. Dual-excitation Algorithm

Consider the magnetic permeability inside the biological tissues to be equal to that in the vacuum. Ampere's Law reads

$$\nabla \times \mathbf{H} = \sigma \mathbf{E} + j\omega\varepsilon\mathbf{E} \tag{1}$$

where $\mathbf{H}$ is the magnetic field strength, $\mathbf{E}$ the electric field vector, ω the operating angular frequency. Using the complex permittivity $\varepsilon_c=\varepsilon-j\sigma/\omega$, taking curl of both hand sides of eq. (1) and substituting with $\nabla \times \mathbf{E} = -j\omega\mu_0\mathbf{H}$, we get its matrix form

$$\begin{bmatrix} -\nabla^2 H_x \\ -\nabla^2 H_y \\ -\nabla^2 H_z \end{bmatrix} = \omega^2\mu_0\varepsilon_c \begin{bmatrix} H_x \\ H_y \\ H_z \end{bmatrix} + j\omega \begin{bmatrix} 0 & E_z & -E_y \\ -E_z & 0 & E_x \\ E_y & -E_x & 0 \end{bmatrix} \begin{bmatrix} \partial\varepsilon_c/\partial x \\ \partial\varepsilon_c/\partial y \\ \partial\varepsilon_c/\partial z \end{bmatrix} \tag{2}$$

According to Ampere's Law, we replace the electric field components with magnetic field components. In addition, we neglect z component of magnetic field (H_z) since it is less

This work was supported in part by NIH R21EB006070, the NNSF of China (50577055), NSF BES-0602957, and the Supercomputing Institute of the University of Minnesota. X.T. Zhang was partly supported by the Lu's Postgraduate Education International Exchange Fund of Zhejiang University.

Xiaotong Zhang is with the University of Minnesota, Minneapolis, MN 55406 USA (e-mail: zhan0709@umn.edu).

Shanan Zhu is with the Zhejiang University, Hangzhou, 310027, China (e-mail: zsa@zju.edu.cn).

Bin He is with the University of Minnesota, Minneapolis, MN 55406 USA (e-mail: binhe@umn.edu).

dominant compared with transverse magnetic field especially within the TEM coil [13]. Then we rewrite the first two lines of eq. (2) below

$$\begin{cases} -\nabla^2 H_x = \omega^2 \mu_0 H_x \varepsilon_c - (\partial H_x / \partial z)[(\partial \varepsilon_c / \partial z)/\varepsilon_c] \\ \qquad + (\partial H_y / \partial x - \partial H_x / \partial y)[(\partial \varepsilon_c / \partial y)/\varepsilon_c] \\ -\nabla^2 H_y = \omega^2 \mu_0 H_y \varepsilon_c - (\partial H_y / \partial z)[(\partial \varepsilon_c / \partial z)/\varepsilon_c] \\ \qquad + (\partial H_y / \partial x - \partial H_x / \partial y)[(\partial \varepsilon_c / \partial x)/\varepsilon_c] \end{cases} \quad (3)$$

In Eq. (3), H_x and H_y distributions correspond to B_1-mapping results, while ε_c, $(\partial \varepsilon_c / \partial x)/\varepsilon_c$, $(\partial \varepsilon_c / \partial y)/\varepsilon_c$ and $(\partial \varepsilon_c / \partial z)/\varepsilon_c$ are unknown. Once we acquire another set of $H_x \sim H_y$ data, we can form a set of linear equations with four equations and four unknown variables, and thus ε_c can be solved. In the present study, we used linear excitation mode to generate different polarizations by switching the current feed point 90° and 30° apart from each other, separately.

In this simulation study, all EM fields were calculated by means of finite element method using software ANSYS 11.0 whereas the postprocessing of EM field data was completed by MATLAB 7.1.

III. Method

A. Finite Element Models

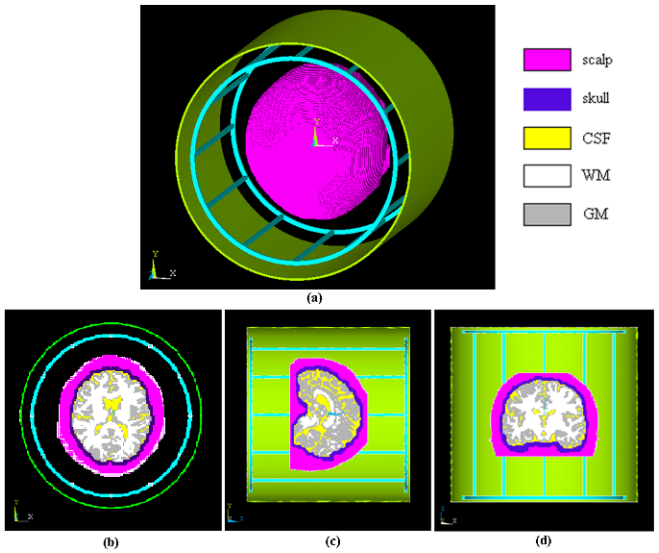

Fig. 1. Overviews (a) and axial (b), sagittal (c) and coronal (d) views of the FEM head and coil models. The head model was meshed with hexahedral element while the coil with tetrahedral element. (green: copper shield, cyan: rungs and end-rings; magenta: scalp, purple: skull, yellow: CSF, white: WM, grey: GM)

T1-weighted MRI images (128×128×72, 2×2×2mm^3) of a human head, which covered the whole brain, have been acquired from a 3T Siemens MRI system. Then the head images were segmented into five tissues: skull, scalp, CSF, WM and GM. These structure information were imported into ANSYS software, and a five-tissue anatomically accurate head model was constructed using hexahedral element with mesh size of 2×2×2mm^3 which is equivalent to the voxel size of MRI images.

A 12-rung birdcage coil and TEM coil were modeled with a diameter of 28cm and a length of 28cm. Either coil was enclosed by a cylindrical shield having a diameter of 32cm and a length of 30cm. Both the coil and the shield were meshed with tetrahedral element and assigned with copper material. Fig. 1 (a) illustrates the FEM models of the head and shielded birdcage coil, and (b)-(d) show the structural views on the axial, sagittal and coronal planes.

To perform a linear excitation, the equivalent circuit model [14] was utilized to calculate the electric current in each rung. All of the capacitors in the coil were replaced with current sources at required resonant frequency.

B. Simulation Protocols

Simulations were conducted in 3T (128MHz) environment. The corresponding EP values for different head tissues were derived from the 4-Cole-Cole Model [15].

In order to test the noise tolerance of the proposed algorithm, we added Gaussian white noise (GWN) to the simulated B_1 field data. The noise level is evaluated by SNR_{B1}, which is defined as follows

$$SNR_{B1} = A / s_{amp} \quad (4)$$

where A is the amplitude of noise-free B_1 field voxel signal, and s_{amp} is the standard deviation (STD) of amplitude noise. The phase noise STD is $s_{phase} = 1/\sqrt{2}\ SNR_{B1}$. In this study, we assumed SNR_{B1}=200.

The Wiener adaptive low-pass filter was applied to pre-process the "contaminated" B_1 maps.

IV. Results

We chose the central slice of the head model to be the imaging plane. Fig. 2 shows the reconstructed results when noise-free and SNR_{B1}=200 using TEM coil and coil excitation S1 and S3. The tissues can be clearly differentiated even with noise added.

We applied S1 and S3, which corresponds to two adjacent rungs as current feed points individually, to excite the TEM coil. In addition, to verify the influence by neglecting H_z component, simulation was also conducted on the birdcage coil model with S1 and S2. Comparison of reconstruction results (noise-free) is described in Fig. 3. With different coil excitation schemes for the TEM coil, reconstruction results are almost the same, which indicate the uniqueness characteristics of our algorithm. With the same excitation scheme but different coils, we observe that for the birdcage coil, reconstruction results differ from that of TEM coil, and the tissues can also be well differentiated, which suggests that neglecting H_z component would insignificantly affect reconstruction results.

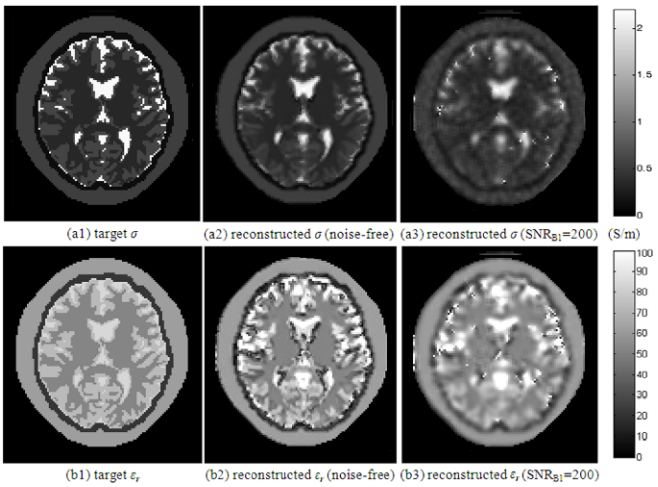

Fig. 2. Reconstructed EPs distribution with the TEM coil when noise-free and SNR_{B1}=200. Coil excitation schemes S1 and S2 were applied (upper row: σ distribution, bottom row: ε_r distribution; from left to right: target EPs, noise-free, SNR_{B1}=200).

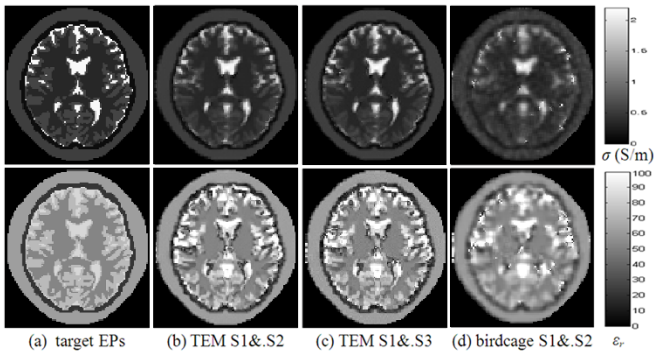

Fig. 3. Reconstruction EPs distribution with two coils and different coil excitation schemes when noise-free (upper row: σ distribution, bottom row: ε_r distribution; from left to right: target EPs, TEM S1&.S2, TEM S1&S3, birdcage S1&S2).

V. Discussion

MREPT promises to be able to reconstruct not only the conductivity distribution, as EIT, MIT, MREIT or MAT-MI aims to do, but also the permittivity distribution within biological tissues, thus enriching our observations of their conditions. In addition, MREPT does not require electrode mounting or external energy deposition which poses a potential safety concern. As our simulation results indicate, the dual-excitation algorithm furnishes us with a practical approach to reconstructing the conductivity and permittivity distributions within a human. The desirable reconstruction results of tissues (Figs. 2 and 3) suggest that MREPT head imaging deserves further investigation and can be extended to other organs of human body.

In our algorithm, the z component of the magnetic field intensity H_z is neglected. The present simulation results suggest our method still works well even in a birdcage coil (Fig. 3), in which H_z component prominently exists and is mainly generated by end-rings. Using a TEM coil, we can get better reconstruction EPs images with higher accuracy.

The uniqueness of solution is an important issue in inverse problems. We applied three coil excitation schemes, and conducted the reconstruction procedures by choosing two 30°-apart (adjacent) and 90°-apart current feed points. It is shown that (Fig. 3), under either excitation combination, our inverse algorithm works well and produces the same EPs distribution, which suggests the uniqueness characteristic of its solution. Besides, these promising results also indicate that, when the switching of current feed point is infeasible, our algorithm may be effective as well by careful subject rotation over a small angle. The theoretical ground of uniqueness of the MREPT imaging problem will need further investigation.

Acknowledgment

We would like to thank Drs. Yiping Du, Zhongmin Liu, and Ulrich Katscher for useful discussions, and Mr. Won Hee Lee for technical assistance in the head FEM modeling.

References

[1] E.C. Fear, X. Li, S.C. Hagness, and M.A. Stuchly, "Confocal microwave imaging for breast cancer detection: localization of tumors in three dimensions," *IEEE Trans. Biomed. Eng.*, vol. 49, (no. 8), pp. 812-22, Aug 2002.

[2] P. Metherall, D.C. Barber, R.H. Smallwood, and B.H. Brown, "Three-dimensional electrical impedance tomography," *Nature*, vol. 380, (no. 6574), pp. 509-12, Apr 11 1996.

[3] H. Griffiths, W.R. Stewart, and W. Gough, "Magnetic induction tomography. A measuring system for biological tissues," *Ann. N Y Acad. Sci.*, vol. 873, pp. 335-45, Apr 20 1999.

[4] H.S. Khang, B.I. Lee, S.H. Oh, E.J. Woo, S.Y. Lee, M.Y. Cho, O. Kwon, J.R. Yoon, and J.K. Seo, "J-substitution algorithm in Magnetic Resonance Electrical Impedance Tomography (MREIT): Phantom experiments for static resistivity images," *IEEE Trans. Med. Imaging*, vol. 21, (no. 6), pp. 695-702, Jun 2002.

[5] M. Joy, G. Scott, and M. Henkelman, "In vivo detection of applied electric currents by magnetic resonance imaging," *Magn. Reson. Imaging.*, vol. 7, (no. 1), pp. 89-94, 1989.

[6] Y. Xu and B. He, "Magnetoacoustic tomography with magnetic induction (MAT-MI)," *Phys. Med. Biol.*, vol. 50, pp. 5175-5187, 2005.

[7] E.M. Haacke, L.S. Petropoulos, E.W. Nilges, and D.H. Wu, "Extraction of conductivity and permittivity using magnetic resonance imaging," *Phys. Med. Biol.*, vol. 38, (no. 6), pp. 723-734, 1991.

[8] H. Wen, "Noninvasive quantitative mapping of conductivity and dielectric distributions using RF wave propagation effects in high-field MRI," *Proc. SPIE*, vol. 5030, pp. 471-477, 2003.

[9] U. Katscher, T. Dorniok, C. Findeklee, P. Vernickel, and K. Nehrke, "In vivo determination of electric conductivity and permittivity using a standard MR system," *13th International Conference on Electrical Bioimpedance and the 8th Conference on Electrical Impedance Tomography*, 2007, pp. 508-511.

[10] S. Akoka, F. Franconi, F. Seguin, and A. Lepape, "Radiofrequency Map of an Nmr Coil by Imaging," *Magn Reson Imaging*, vol. 11, (no. 3), pp. 437-441, 1993.

[11] J.H. Wang, M.L. Qiu, Q.X. Yang, M.B. Smith, and R.T. Constable, "Measurement and correction of transmitter and receiver induced nonuniformities in vivo," *Magn. Reson. Med.*, vol. 53, (no. 2), pp. 408-417, Feb 2005.

[12] D.I. Hoult, "The principle of reciprocity in signal strength calculations - A mathematical guide," *Conc. Mag. Res.*, vol. 12, (no. 4), pp. 173-187, 2000.

[13] J.T. Vaughan, G. Adriany, C.J. Snyder, J. Tian, T. Thiel, L. Bolinger, H. Liu, L. DelaBarre, and K. Ugurbil, "Efficient high-frequency body coil for high-field MRI," *Magn. Reson. Med.*, vol. 52, (no. 4), pp. 851-859, Oct 2004.

[14] J.M. Jin, *Electromagnetic Analysis and Design in Magnetic Resonance Imaging*, New York: CRC Press, 1999.

[15] S. Gabriel, R.W. Lau, and C. Gabriel, "The dielectric properties of biological tissues: III. Parametric models for the dielectric spectrum of tissues," *Phys. Med. Biol.*, vol. 41, (no. 11), pp. 2271-93, Nov 1996.